Original Article

Combining and analyzing novel multi-parametric magnetic resonance imaging metrics for predicting Gleason score

Rulon Mayer[1,2], Baris Turkbey[3], Peter Choyke[3], Charles B. Simone II[4]

[1]University of Pennsylvania, Philadelphia, PA, USA; [2]OncoScore, Garrett Park, MD, USA; [3]National Institutes of Health, Bethesda, MD, USA; [4]New York Proton Center, New York, NY, USA

Contributions: (I) Conception and design: R Mayer; (II) Administrative support: R Mayer, CB Simone 2nd, P Choyke; (III) Provision of study materials or patients: B Turkbey, P Choyke; (IV) Collection and assembly of data: R Mayer, B Turkbey, P Choyke; (V) Data analysis and interpretation: R Mayer; (VI) Manuscript writing: All authors; (VII) Final approval of manuscript: All authors.

Correspondence to: Rulon Mayer, PhD. University of Pennsylvania, Philadelphia, PA 19104, USA; OncoScore, Garrett Park, MD 20896, USA. Email: mayerru@yahoo.com.

Background: Radiologists currently subjectively examine multi-parametric magnetic resonance imaging (MP-MRI) to determine prostate tumor aggressiveness using the Prostate Imaging Reporting and Data System scoring system (PI-RADS). Recent studies showed that modified signal to clutter ratio (SCR), tumor volume, and eccentricity (elongation or roundness) of prostate tumors correlated with Gleason score (GS). No previous studies have combined the prostate tumor's shape, SCR, tumor volume, in order to predict potential tumor aggressiveness and GS.

Methods: MP-MRI (T1, T2, diffusion, dynamic contrast-enhanced images) were obtained, resized, translated, and stitched to form spatially registered multi-parametric cubes. Multi-parametric signatures that characterize prostate tumors were inserted into a target detection algorithm [adaptive cosine estimator (ACE)]. Pixel-based blobbing, and labeling were applied to the threshold ACE images. Eccentricity calculation used moments of inertia from the blobs. Tumor volume was computed by counting pixels within multi parametric MRI blobs and tumor outlines based on pathologist assessment of whole mount histology. Pathology assessment of GS was performed on whole mount prostatectomy. The covariance matrix and mean of normal tissue background was computed from normal prostate. Using signatures and normal tissue statistics, the z-score, noise corrected SCR [principal component (PC), modified regularization] from each patient was computed. Eccentricity, tumor volume, and SCR were fitted to GS. Analysis of variance assesses the relationship among the variables.

Results: A multivariate analysis generated correlation coefficient (0.60 to 0.784) and P value (0.00741 to <0.0001) from fitting two sets of independent variates, namely, tumor eccentricity (the eccentricity for the largest blob, weighted average for the eccentricity) and SCR (removing 3 PCs, removing 4 PCs, modified regularization, and z-score) to GS. The eccentricity t-statistic exceeded the SCR t-statistic. The three-variable fit to GS using tumor volume (histology, MRI) yielded correlation coefficients ranging from 0.724 to 0.819 (P value <<0.05). Tumor volumes generated from histology yielded higher correlation coefficients than MRI volumes. Adding volume to eccentricity and SCR adds little improvement for fitting GS due to higher correlation coefficients among independent variables and little additional, independent information.

Conclusions: Combining prostate tumors eccentricity with SCR relatively highly correlates with GS.

Keywords: Tumor morphology; prostate cancer; multi-parametric magnetic resonance imaging (MP-MRI); Gleason score (GS); histology of whole mount prostatectomy; signal to clutter ratio (SCR); regularization

Submitted Dec 15, 2021. Accepted for publication Apr 08, 2022.
doi: 10.21037/qims-21-1092
View this article at: https://dx.doi.org/10.21037/qims-21-1092

Introduction

Upon detecting prostate cancer, clinical management requires deciding whether to monitor (1) or treat prostate cancer. The therapy, whether with surgery or radiation, can impose great physical and psychological burdens on the patient that maybe especially troublesome if unnecessary. However, mistakenly assessing the prostate cancer to be benign rather than malignant can result in metastases, severe suffering from the effects of progressive disease, and death. A number of tools (2-6) have been developed to make the critical assessment of biologic aggressiveness of prostate cancer. Although determination of prostate serum antigen (PSA) levels in the blood specimen sometimes provides an important, non-invasive guide for patient management. PSA is not well correlated with actual patient status (7-9). Meta-data (6) such as age, family history, diet, can also contribute and aid assessment of a patient's tumor status. The best predictor for disease progression is determination of the Gleason score (GS) (10) derived from a pathologist's microscopic examination of the stained biopsy or whole mount prostatectomy sections. However, extracting tumor samples with a biopsy or a whole mount prostatectomy burdens the patient with an invasive procedure and can also generate inaccurate readings due to sampling error. Therefore, an entirely non-invasive method of assessing tumor aggressiveness would be ideal.

For such a non-invasive biomarker to be useful, it is crucially important to develop a reliable, non-invasive, quantitative predictor of tumor progression. Examining magnetic resonance imaging (MRI) images (11-15) of prostate cancer patients provides an opportunity to assess tumor aggressiveness. In particular, trained radiologists visually examine a number of types of MRI sequences [often referred to as multi-parametric or multi-parametric magnetic resonance imaging (MP-MRI)] and follow proscribed rules to determine prostate tumor status following the Prostate Imaging-Reporting and Data System (PI-RADS) protocol (11). Currently research (11) employing the PI-RADS approach also is predictive of lymph node involvement, extra-prostatic extension, and clinically significant disease (13), but only weakly correlates with GS (14). Due to its subjective nature, the PI-RADS approach is vulnerable to inter-reader variability especially with inexperienced radiologist's interpretations of the MRI (16). A quantitative, objective approach could support and guide the clinical impact of MRI.

Recently, supervised algorithms were modified and applied to spatially registered MP-MRI of prostate tumors (17-21). These algorithms used in-scene and transformed tumor signatures (17) to infer the GS. Analysis of the prostate tumors from the spatially registered MP-MRI determined prostate tumor characteristics such as volume (18), eccentricity (or shape) (19) derived from histology of whole mount prostatectomy and MP-MRI and signal to clutter ratio (SCR) or Z-score taken from MP-MRI. Earlier work then examined the correlation of the GS with tumor volume (20), tumor eccentricity (19), a modified tumor SCR (21), and novel tumor eccentricity predicted GS better than the more conventional tumor volume (20). This study extends the examination of the MP-MRI metrics and GS and assesses combining two (eccentricity, SCR) or three (volume, eccentricity, SCR) variables to predict GS. To see if each independent variable (volume, eccentricity, and SCR) adds significant new information to fitting the GS, the relationship and correlation coefficients among the independent variables is also computed and analyzed.

The present paper is the first and only study to combine a modified SCR (21) and another novel metric eccentricity (19), and their possible relationship with GS. The computation of filtered and regularized SCR (21) and their relationship with GS was first presented and examined in 2021. The relationship between eccentricity and GS first presented and examined in 2021. Following validation from more independent studies and greater patient numbers, employing novel noninvasive MRI indicators of disease status (including ones not considered in this study) and a predictive model for GS will hopefully generate a digital nomogram and elevate and simplify patient management. We present the following article in accordance with the TRIPOD reporting checklist (available at https://qims.amegroups.com/article/view/10.21037/qims-21-1092/rc).

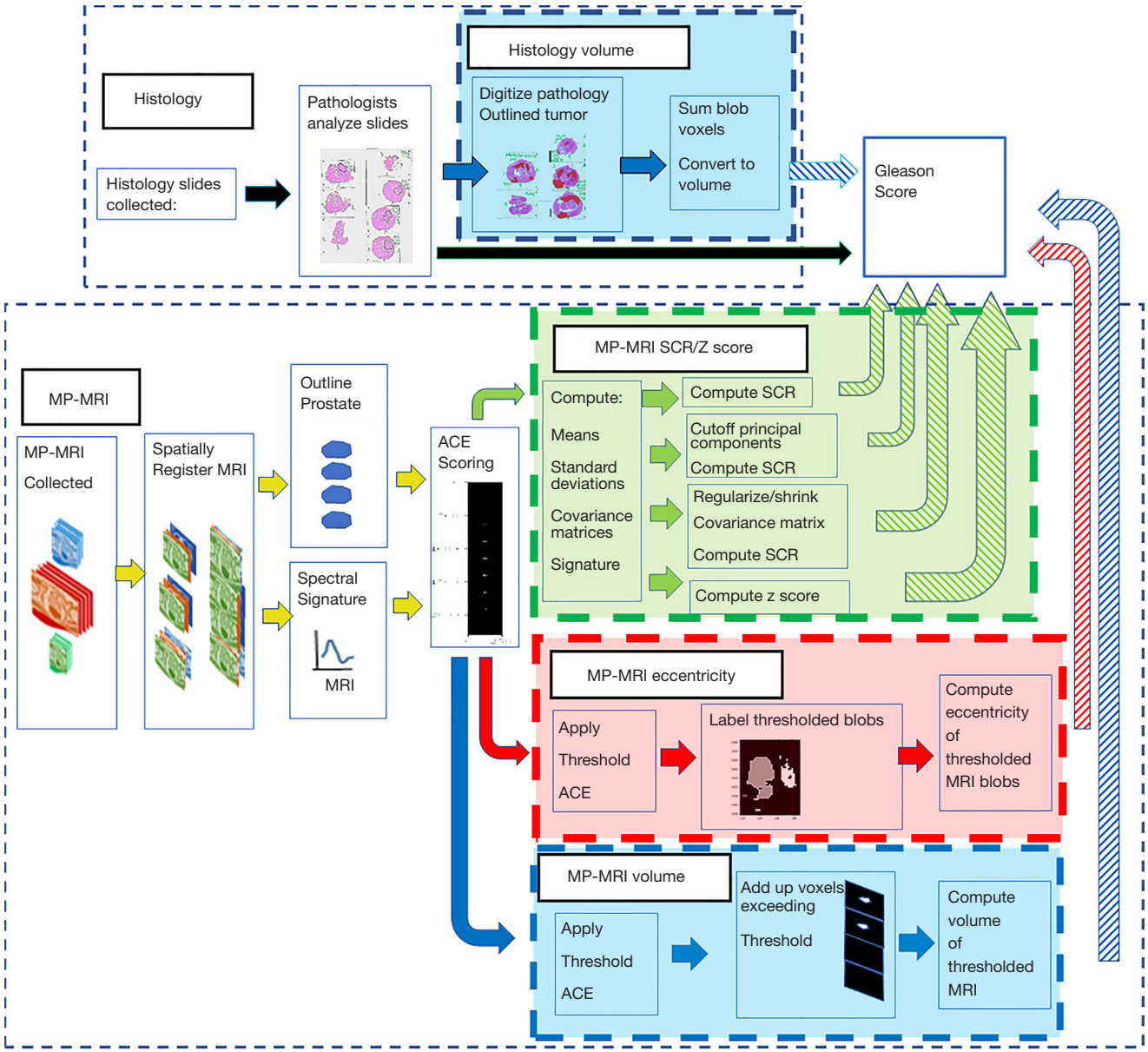

Figure 1 Overall method scheme for fitting Gleason score (histology of whole mount prostatectomy) from MP-MRI derived eccentricity (red), MP-MRI derived SCR (green), volume from histology and MP-MRI (blue). MP-MRI, multi-parametric magnetic resonance imaging; SCR, signal to clutter ratio; ACE, adaptive cosine estimator.

Methods

Overall description of histology and MP-MRI determination

This study followed a number of tracks (*Figure 1*) (18,19,21) to determine the relationship between prostate tumor morphology (eccentricity), tumor volume, and tumor SCR, and GS. Spatially registered hypercubes were resized, translated, and stitched together (yellow arrows, highlight) from the patient's MP-MRI (17). Another track (18) (blue arrows, highlight) estimated the tumor volume from histology and MP-MRI using supervised target detection. One track (red arrows, highlight) computed the tumors eccentricity (19) for supervised target analysis applied to MP-MRI. The other track (green arrows, highlight) computed the SCR (21) applied to spatially registered

multi-parametric MRI. The GS was determined by a pathologist analyzing histology slides derived from whole mount prostatectomy from tumors. This study analyzed 25 of 26 consecutive patients that had underwent radical prostatectomy. Only one of the 26 patients was not analyzed due to failure to show contrast uptake in the MRI dynamic contrast enhancement images. GS was denoted as the dependent variable (solid black arrow in *Figure 1*) (17). The eccentricity (19), tumor volume (20), and SCR (21) were treated as the independent variables in multi-variate regression fitted calculations. The eccentricity (19) was determined from manipulating the computed moments of inertia for voxels inside a blob. Tumor volume (20) was derived from threshold adaptive cosine estimator (ACE) applied to the hyperspectral images. SCR (21) was generated from tumor signatures and statistics of the normal prostate. Each feature contains candidate metrics, such as filtered and regularized SCR for example. This study examined a variety of possible combinations of components of the independent variables to find an optimal fit to the GS. The tumor eccentricity, SCR, volume was then compared (green, red, blue striped arrows, respectively, in *Figure 1*) to the GS of the tumor. Computation of all features (eccentricity, tumor volume, SCR) used custom software written in Python 3.6 and 3.7. Multiple regression affiliated metrics such as t-values, P values, Shapiro-Wilks etc. used Statsmodel, a Python module.

Study design and population

The Cancer Imaging Archive (TCIA) (22,23), affiliated with The National Institutes of Health (NIH), collected and stored the patient data from prostate tumor MRI and histology from whole mount prostatectomy specimens. The study was conducted in accordance with the Declaration of Helsinki (as revised in 2013). This retrospectively designed, single institution study was approved by the NIH Institutional Review Board, and was compliant with the Health Insurance Portability and Accountability Act. Individual consent for this retrospective analysis was waived. All cases were anonymized. A total of 26 patients were included. All patients had biopsy proven adenocarcinoma of the prostate, with median patient age 60 years (range, 49 to 75 years), with median PSA 5.8 ng/mL (range, 2.3 to 23.7 ng/mL), and with median GS 7 (range, 6 to 9). Eighteen of the 26 patients had tumor size >1 cc. This study placed no restrictions on tumor location within the prostate. Robotic assisted radical prostatectomy was performed at a median time of 60 days (minimum 3 days, maximum 180 days) following MRI without any intervening treatment.

Whole mount prostatectomy and histology

The whole mount prostatectomy histology has previously been described in great detail and is very briefly summarized (24-26). Following radical prostatectomy, the specimen was fixed at room temperature in formalin for 2 to 24 h, and then placed in the customized 3D mold and sliced in sections with a separation of 6 mm. in the axial direction, corresponding to the MRI axial plane section. The individual tumor foci, dimensions, and GSs from the histology slides were independently determined by two experienced pathologists, blinded to the MRI results. As in previous efforts (17-21) and to better reflect the patient's status, a patient's GS was a weighted average (based on histology blob size) of the GSs assessed by the pathologist. The tumor's shape (or eccentricity) and tumor volume from histology slides of sectioned whole mount prostatectomy was determined from analysis of the digitized version of the pathology delineated marks of the tumor, and computed using Eqs. [2-5].

Magnetic resonance imaging

The MRI collection was composed of diffusion weighted images (DWIs), dynamic contrast enhanced (DCE), and structural (T1, T2) images. The pulse sequences were described in earlier studies (24-26). Triplanar T2W turbo spin echo, DW MRI, and axial pre-contrast T1-weighted axial 3D fast field echo DCE MRI sequences, were part of this MRI protocol. A prior study (26) described their detailed sequence parameters. The mean interval between MRI and radical prostatectomy was 60 days (range, 3 to 180 days).

Image processing, pre-analysis

DCE are formed from a time series of images. These images display the evolution in time of contrast material over several hundred s following injection. The DCE shows the contrast uptake in the tissues. By analyzing the DCE and exploiting the unique tumor physiology, a portion of tumors may be identified. The tracer concentration in the tissue that supplies and empties through the tumor vasculature is described by a simple two compartment model (17,27,28). For times greater (>50 s), than the time to reach the peak uptake of the contrast material in a tumor, every voxel was

fitted with an exponentially decaying function to form the washout (k_{ep}) images and the probability likelihood (prob) images.

The MRI images were digitally resized (17-21) to 1 mm resolution in the transverse direction. Using the known location of patient's table position, the slices were resized to 6 mm spacing and aligned using resampling. Due to the short time intervals between scans (<20 minutes), small rigid adjustments (minor transverse translation) were applied to the structural, diffusion, and DCE images. A "cube" is composed of stacked individual slices were scaled, translated, resliced so as to be spatially registered at the pixel level. These "three dimensional" (two transverse directions plus spectral composed of MP-MRI modalities) cubes were "stitched" together into a narrow three-dimensional hypercube to depict the entire MRI scan. The spectral content of the hypercube had 7 components (17-21) [T1 (pre contrast), T1 (maximum contrast), T2, ADC, DWI-high B (B=1,000 s/mm^2), Washout or k_{ep} from DCE].

ACE

The ACE (Eq. [1]) (29-31) was transferred for this medical application (17-21) and applied to spatially registered MP-MRI. The algorithm (ACE) uses in-scene multispectral tumor signatures (for tumor). S is the target (tumor) signature and is a 7-component vector [DWI, T1, T2, ADC, DCE in this analysis (17-21)]. S, the in-scene tumor signature, is selected from yellow voxels in a three-color display of the spatially-registered MP-MRI (red is Washout, green is DWI, high-B, blue is ADC) (17-21). The component S_q (for vector S) is the average from T target vector-voxels $x_{p,q}$ summed over p target voxels (identified as yellow) (see Eq. [1]). μ is the background (normal prostate) 7 component vector. CM is the covariance (7×7) matrix for the background. The background voxels needed for μ and CM were taken from digitally outlining the prostate on the spatially-registered MP-MRI (17-21).

$$S_q = \frac{1}{T}\sum_{p=1}^{T} x_{p.q}, \quad \mu_q = \frac{1}{N}\sum_{p=1}^{N} x_{p.q},$$
$$ACE(x_i) = \frac{(S-\mu)^T CM^{-1}(x_i-\mu)}{\sqrt{\left[(S-\mu)^T CM^{-1}(S-\mu)\right]\left[(x_i-\mu)^T CM^{-1}(x_i-\mu)\right]}} \quad [1]$$

To compute the background statistics, the prostate image is manually outlined for all slices to generate an image mask and restrict computations to the prostate volume. ACE generates a conical hyperspace decision surface. A large angle (but small cosine, small ACE score, outside decision cone) or a small angle (but large cosine, large ACE score, inside the decision cone) determines whether a voxel is background (normal tissue) or target (tumor).

Labeling and blob generation

Blobbing and labeling (19) aggregate neighboring pixels. The blobbing is applied to a binary image following application of a threshold to the primary image. Binary tumor masks are generated from digitized maps of tumor outlines marked by pathologists on histology slides. In addition, binary masks were derived from the pixels that exceed a threshold of ACE target detection applied to MP-MRI hypercubes. Each pixel is perused within a given neighborhood to determine if they are a blob candidate. If the pixels are deemed to be a blob member, then they are connected, collected, and labeled as a member of a particular blob.

Eccentricity calculation

Custom software (coded in Python 3) was used to calculate the eccentricity and volume (19) for every labeled blob. The moment of inertia matrix I for the kth blob was computed. From the eigenvalues of the moment of inertia I, the largest eigenvalue was assigned to the large axis l_k and the second minor axis eigenvalue was assigned to the transverse moment s_k. The eccentricity E_k for the kth blob with a major axis l_k and minor axis s_k is given by

$$E_k = \frac{l_k - s_k}{s_k} \quad [2]$$

Eccentricity values E_k range from 0 to 1. A spherical shape has an eccentricity E_k of 0. A line has an eccentricity E_k of 1. Each blob's volume V_k is given total number of pixels within each blob and corrected by the voxel volume r (assuming density of unity for each voxel),

$$V_k = rN = r\sum_{i=1}^{N} \frac{x_i}{abs(x_i)} \quad [3]$$

and r is the total volumetric resolution (6 mm^3 per voxel for MP-MRI and 0.00270 mm^3 per voxel for the histology

slices in this study).

The weighted eccentricity W is sum over B blobs, and is given by

$$W = \frac{\sum_{k=1}^{B} V_k E_k}{\sum_{k=1}^{B} V_k} \quad [4]$$

Overall quantitative metrics description: z-score and SCR

Z-score is a quantitative metric (32) for assessing the degree of disease. It is computed using the digital values from MRI. The z_score for given for each modality q is (32):

$$z\_score_q = \left(\frac{S_q - \mu_q}{\sigma_q} \right)^2 \quad [5]$$

and q ranges from q=1,2,3…M (M=7 in this study), where S_q is the tumor signature (Eq. [1]) or value in the modality q (mean over the T tumor pixels), μ_q is the mean value for normal prostate in MRI modality q (Eq. [1]),

$$\sigma_q = \frac{1}{N} \left(\sum_{p=1}^{N} \left(x_{p,q} - \mu_q \right)^2 \right)^{1/2} \quad [6]$$

σ_q is the standard deviation for the normal prostate in modality q, and p ranges over all N prostate voxels. The background voxels needed for μ and CM were taken from digitally outlining the prostate on the spatially-registered MP-MRI. A simple way of combining all M MRI modalities q is to sum the individual z-score$_i$, i.e.,

$$z\_score = \sum_{q=1}^{M} z\_score_q \quad [7]$$

The SCR (21,29-31) is given by

$$SCR = \left(S - \mu \right)^T CM^{-1} \left(S - \mu \right) \quad [8]$$

that is a matrix multiplication over MP-MRI modalities, the superscript T denotes a vector transpose operation, CM is the covariance matrix, and the superscript –1 denotes a matrix inverse operation.

Filtering noise

The inverse covariance matrix CM^{-1} is a square symmetrical matrix and decomposes into three parts (33),

$$CM^{-1} = \Lambda^T \lambda^{-1} \Lambda \quad [9]$$

namely the eigenmatrix Λ, transpose of the eigenmatrix Λ^T, and diagonal matrix λ with eigenvalues λ_1^2, λ_2^2, $\lambda_3^2 \ldots \lambda_M^2$ populating the diagonal

$$\lambda^{-1} = \begin{bmatrix} \frac{1}{\lambda_1^2} & 0 & .... & 0 & 0 \\ 0 & \frac{1}{\lambda_2^2} & & & 0 \\ ... & & ... & & ... \\ 0 & & & \frac{1}{\lambda_{M-1}^2} & 0 \\ 0 & 0 & ... & 0 & \frac{1}{\lambda_M^2} \end{bmatrix} \quad [10]$$

The eigenvalues are ordered according to size ranging from the largest λ_1 to the smallest λ_M. The images corresponding to the eigenvalues and eigenvectors and principal components (PCs) range from high signal and variation (1,2) to low variation and very noisy (M–1, M). The lowest value PCs (M–1, M) elevate the noise due to the inversion in the inverse matrix CM^{-1} (Eq. [9]). Filtering out the noisy PCs (21,34,35) means removing or deleting the lowest valued eigenvalues (3 or 4 in this study) from the inverse matrix, i.e.,

$$\lambda_{Filtered}^{-1} = \begin{bmatrix} \frac{1}{\lambda_1^2} & 0 & & 0 & 0 \\ 0 & \frac{1}{\lambda_2^2} & & & 0 \\ ... & & ... & & ... \\ 0 & & & 0 & 0 \\ 0 & 0 & ... & 0 & 0 \end{bmatrix} \quad [11]$$

and inserting Eq. [11] into Eq. [9]

$$CM_{Filtered} = \Lambda^T \lambda_{Filtered}^{-1} \Lambda \quad [12]$$

resulting in

$$SCR_{Filtered} = (S-\mu)^T CM_{Filtered}^{-1} (S-\mu) \quad [13]$$

after inserting Eq. [10] into Eq. [8].

Regularization and shrinkage

The goal of shrinkage regularization (21,35) is to perturb the covariance matrix CM(γ) to maximize the likelihood estimation, or equivalently minimize the discriminant function d(γ) [=-ln(normal distribution)] by adding a diagonal component that is controlled by the parameter γ and thereby perturbing the covariance matrix CM into the regularized $CM_{mod\_Reg}(\gamma)$

$$CM_{mod\_Reg} = (1-\gamma)CM + \gamma V \quad [14]$$

V is a diagonal matrix filled up with the square of the standard deviations from M modalities is given by

$$V = \begin{bmatrix} \sigma_1^2 & 0 & & 0 & 0 \\ 0 & \sigma_2^2 & & & 0 \\ \ldots & & \ldots. & & \ldots \\ 0 & & & \sigma_{M-1}^2 & 0 \\ 0 & 0 & \ldots. & 0 & \sigma_M^2 \end{bmatrix} \quad [15]$$

Using Eqs. [14-15] the modified discriminant function $d_{mod\_Reg}(\gamma)$

$$d_{mod\_Reg}(\gamma) = \sum_{i=1}^{N} (x_i-\mu)^T CM_{mod\_Reg}^{-1}(\gamma)(x_i-\mu) + \ln\left(\det\left(CM_{mod\_Reg}(\gamma)\right)\right) \quad [16]$$

is computed for $0<\gamma<1$ and a minimum $d_{mod}(\gamma_{min})$ is found at $\gamma_{min.}$ resulting in a SCR_{Mod_Reg} (Eq. [17]) using a modified regularization procedure (using Eqs. [14-16]).

$$SCR_{mod\_Reg}(\gamma=\gamma_{min}) = (S-\mu)^T CM_{mod\_Reg}^{-1}(S-\mu) \quad [17]$$

Tumor volume measurements, supervised target detection

Tumor volume from histology determination was derived directly from tumors outlined by a pathologist on slides (18). Tumor volume was given by digitally tracing the tumor on all slices, summing the number of voxels within the pathologist's outline and converting the number of voxels to volume from the image spatial resolution. The transverse spatial resolution (300 dots per inch) for the volume calculation and the histology slice separation (6 mm) resulting in a voxel volume r=4.30×10^{-5} cm^3.

The procedure for estimating the tumor volume using the supervised target detection algorithm or ACE has been previously described (18). For spatially-registered MP-MRI threshold is applied to the ACE map. Voxels exceeding a threshold for ACE scores are assigned to tumor and normal tissue assigned to ACE scores residing below the threshold. The chosen threshold in this study was from 0.40 to 0.85 assessed in 0.05 increments. The number of tumor voxels are converted to volume based on the MRI spatial resolution (1 mm × 1 mm) and slice separation (6 mm) resulting in a voxel volume (r=0.006 cm^3).

Statistics and univariate and multivariate fitting

A multivariate fit (36-39) was applied to the GS, eccentricity, and volume measurements i.e.,

$$GS = b\_const + b\_Ecc*Ecc + b\_SCR*SCR + \varepsilon \quad [18]$$

$$GS = b\_const + b\_Ecc*Ecc + b\_SCR*SCR + b\_Vol*Vol + \varepsilon \quad [19]$$

The GS derived from the pathological assessment of histology slides from prostatectomy were fitted through linear regression with eccentricity (Ecc), SCR, and volume (Vol). Optimal coefficients b_const, b_Ecc, b_SCR, b_Vol or constant, eccentricity coefficient, SCR, volume coefficients respectively, were chosen by minimizing the error ε through the least-squares formulation. Ecc includes Eccentricity from the largest blob using ACE thresholds of 0.35, 0.40, 0.45, eccentricity of the weighted average using ACE threshold of 0.40. SCR includes cutoff from three and four PCs, modified registration, and Z-score. Volume includes histology from whole mount prostatectomy and MP-MRI using ACE thresholds of 0.60, 0.65, 0.70. The Pearson correlation coefficient R, R squared (r squared), adjusted correlation coefficient, t-value, P value, that assess the fitness and probability that the fit departs from null fit, were computed. In addition (36-39), the quality of fit was assessed by computing the F-value and affiliated P value.

To examine if the independent variables (volume,

Table 1 Summary of eccentricity and SCR fit to Gleason score

Two variate metrics	Max Blob: 0.35	Max Blob: 0.4				Weighted: 0.4
	Cutoff: 3 Deleted	Cutoff: 3 Deleted	Cutoff: 4 Deleted	SCR (dB): Mod Regular	Z Score	Cutoff: 3 Deleted
R	0.763	0.784	0.71	0.701	0.696	0.6
R^2	0.582	0.614	0.504	0.491	0.485	0.36
R^2 adjusted	0.544	0.579	0.459	0.445	0.438	0.302
F value	15.323	17.488	11.189	10.623	10.353	6.18
P value	0.00007	0.00003	0.00044	0.00059	0.00068	0.00741
D-P Omni	0.671	0.924	3.578	1.7	2.963	2.399
D-P Omni P value	0.715	0.63	0.167	0.427	0.227	0.301
S-W	0.956	0.948	0.922	0.947	0.916	0.947
S-W P value	0.335	0.222	0.057	0.22	0.042	0.214
b_Ecc	–2.546	–2.728	–2.599	–2.379	–2.483	–2.977
std error	0.607	0.598	0.701	0.77	0.754	1.521
t_Ecc	–4.193	–4.564	–3.707	–3.088	–3.292	–1.958
P value	0.00038	0.00015	0.00123	0.00537	0.00332	0.0631
b_SCR	0.044	0.04	0.029	0.039	0.158	0.046
std error	0.013	0.012	0.016	0.025	0.106	0.016
t_SCR	3.448	3.21	1.778	1.587	1.488	2.893
P value	0.00229	0.00404	0.08926	0.12673	0.15104	0.00845

SCR, signal to clutter ratio; Max Blob, largest blob; Weighted, weighted eccentricity; Cutoff, principal component filtering; 3 Deleted, 3 principal component deleted; 4 Delete, 4 principal component deleted; Mod Regular, modified regularization; MP-MRI, multi-parametric magnetic resonance imaging; R, correlation coefficient; R^2, R squared; R^2 adjust, adjusted R squared; D-P Omni, D'Agostino-Pearson Omnibus residual normality test; S-W, Shapiro-Wilks residual normality test; b_Ecc, eccentricity coefficient; std error, standard error; t_Ecc, eccentricity *t*-value; b_SCR, SCR coefficient; t_SCR, SCR *t*-value.

eccentricity, and SCR) add significant information to the GS fit, the relationship and correlation coefficients among the independent variables is computed and analyzed. Low values of correlation coefficients indicate that the independent variables are truly independent, are not redundant and meaningfully contribute to the GS fit.

D'Agostino-Pearson (D-P) Omnibus and the Shapiro-Wilks (S-W) tests (36-39) generated P values for the null hypothesis of fitted residuals following the normal distribution. The P values for null hypothesis that the residuals' follow homoscedasticity are calculated through the Breusch-Pagan (B-P) test (36-39).

Results

Table 1 summarizes metrics for assessing the multivariate fits (Eq. [18]) for MP-MRI-based eccentricity and SCR measurements to GS. The two sets of independent variables use combinations of prostate tumor eccentricity and SCR. Eccentricity and SCR related topics and results are summarized and listed in *Table 1*. Options and results for b_Ecc include the eccentricity for the largest blob, weighted average for the eccentricity. Options for b_SCR include the cutoff for 3 PCs, cutoff for 4 PCs, modified regularization, and z-score. The fitted coefficients for the eccentricity and SCR b_Ecc and b_SCR are shown along

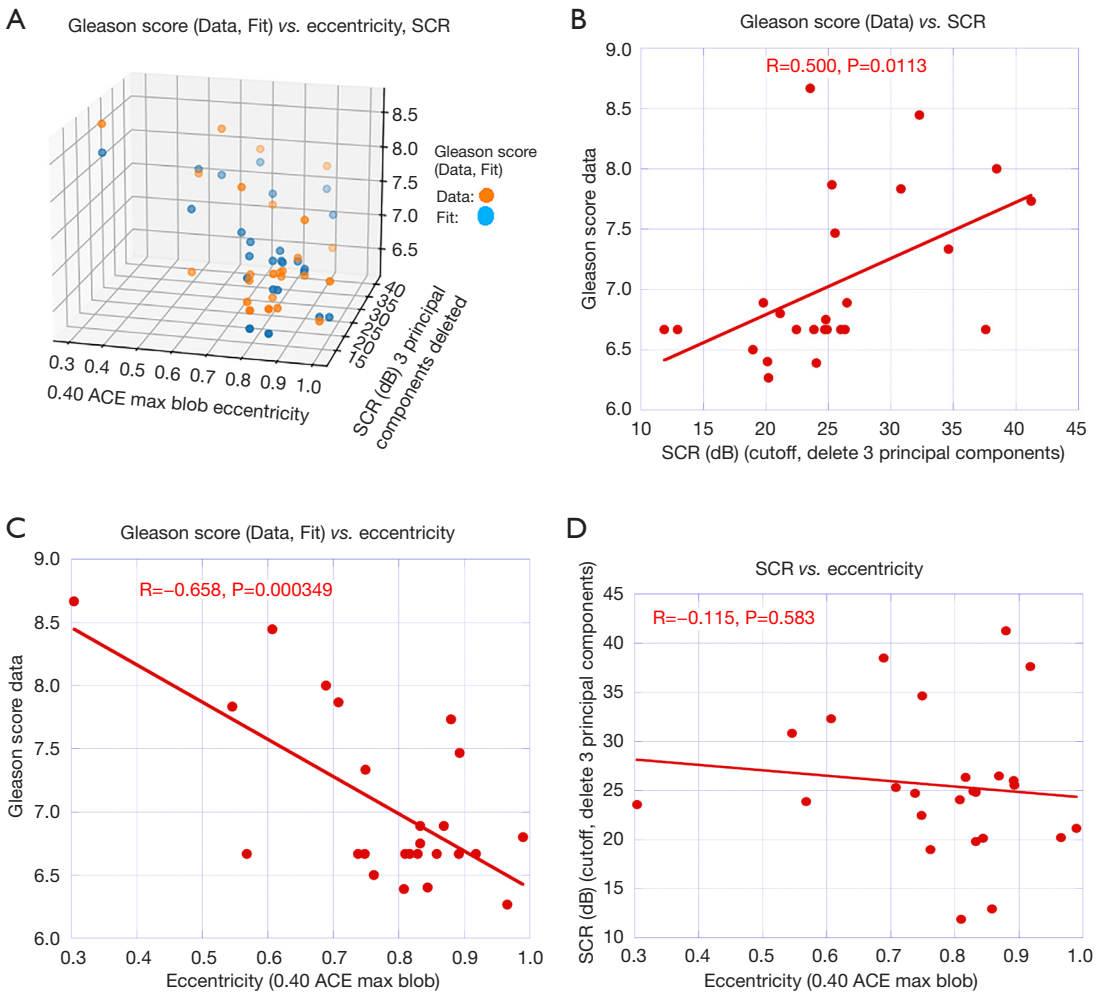

Figure 2 The relationship between Gleason score and eccentricity and SCR. (A) A three-dimensional plot where the orange dots denote the data and the blue dots show the fit; (B) the plot of the Gleason score against the SCR (filtered out 3 principal components); (C) the plot of the Gleason score against the eccentricity (largest blob, ACE threshold =0.40); (D) the plot of the SCR [largest blob, ACE threshold is 0.40] against the eccentricity (largest blob, ACE threshold =0.40). SCR, signal to clutter ratio; ACE, adaptive cosine estimator.

with the standard error for each parameter associated with the fit. The b_Ecc is negative, demonstrating that GS is associated with smaller and more spherical tumors. The b_SCR is positive, confirming that larger departures of MP-MRI from normal prostate are associated with GS. The t statistics for eccentricity t_Ecc and SCR and t_SCR along with P values are displayed in *Table 1*. The magnitude of the t-value t_Ecc is comparable to the t-value t_SCR for all pairs of independent variables. A specific example taken from *Table 1* shows Eccentricity (Maximum Blob Volume, ACE threshold 0.40) yields t_Ecc =−4.56 and SCR with 3 PCs cutoff t_SCR =3.21. Correlation coefficient (R), R squared (R^2), adjusted R squared (R^2 adjusted), F-statistic and P value summarize the overall multivariate fit for MP-MRI-based measurements to GS (Eq. [18]).

Table 1, displays the correlation coefficient R and P value from fitting two sets of independent variates in a multivariate analysis (Eq. [8]) for GS ranged from R=0.60 to 0.784 and P value 0.00741 to <0.0001, respectively. The t-statistic for the eccentricity is comparable to those from SCR measurements. This MP-MRI analysis processed the 25 patients that took up the contrast material. The residuals in the fits mostly followed a normal distribution as evidenced by the P values for the D'Agostino-Pearson and Shapiro-Wilks tests yielding P values >0.05. The residuals in the fits also followed homoscedasticity as shown by

Table 2 Summary of eccentricity, SCR, volume fit to Gleason score

Three variate metrics	Max Blob: 0.35	Max Blob: 0.4	Max Blob: 0.45	Max Blob: 0.4							Weighted: 0.4
	Cutoff: 3 Deleted	Cutoff: 3 Deleted	Cutoff: 3 Deleted	Cutoff: 3 Deleted	Cutoff: 3 Deleted	Cutoff: 3 Deleted	Cutoff: 4 Deleted	Cutoff: 4 Deleted	SCR (dB): Mod Regular	Z Score	Cutoff: 3 Deleted
	Histology	Histology	Histology	MP-MRI: 0.6	MP-MRI: 0.65	MP-MRI: 0.7	Histology	MP-MRI: 0.65	Histology	Histology	Histology
R	0.795	0.819	0.792	0.791	0.800	0.784	0.778	0.726	0.767	0.783	0.724
R^2	0.632	0.670	0.627	0.626	0.641	0.615	0.605	0.527	0.589	0.613	0.524
R^2 adjusted	0.579	0.623	0.574	0.573	0.589	0.560	0.548	0.459	0.531	0.558	0.456
F value	12.01	14.21	11.77	11.74	12.47	11.20	10.71	7.787	10.05	11.11	7.695
P value	8.59e-05	2.79e-05	9.79e-05	9.93e-05	6.70e-05	0.000134	0.000177	0.00111	0.000261	0.000141	0.00118
D-P Omni	2.734	0.772	1.064	0.092	0.67	0.328	0.924	1.228	1.063	0.359	2.931
D-P Omni P value	0.255	0.68	0.587	0.955	0.715	0.849	0.63	0.541	0.588	0.836	0.231
S-W	0.967	0.976	0.962	0.96	0.955	0.965	0.966	0.949	0.965	0.968	0.956
S-W P value	0.563	0.805	0.466	0.415	0.33	0.527	0.544	0.237	0.521	0.593	0.334
b_Ecc	–0.441	–0.4819	–0.4235	–0.531	–5.141	–0.5877	–0.3999	–0.4767	–0.3496	–0.3152	–0.1906
std error	0.156	0.143	0.153	0.163	0.152	–0.154	0.163	0.150	0.178	0.174	0.160
t_Ecc	–2.829	–3.371	–2.763	–3.253	–3.382	–3.813	–2.456	–2.540	–1.969	–1.807	–1.193
P value	0.010	0.003	0.012	0.004	0.003	0.001	0.023	0.0.019	0.062	0.085	0.246
b_SCR	0.431	0.3915	0.3669	0.469	0.4774	0.4325	0.3001	0.3437	0.2935	0.3406	0.4136
std error	0.135	0.128	0.136	0.143	0.138	0.137	0.143	0.170	0.158	0.153	0.154
t_SCR	3.189	3.066	2.691	3.285	3.472	3.155	2.094	2.025	1.853	2.225	2.694
P value	0.004	0.006	0.014	0.004	0.002	0.005	0.049	0.056	0.078	0.037	0.014
b_Vol	0.2665	0.2731	0.3030	0.1401	0.1924	0.0448	0.3621	0.1830	0.3576	0.4192	0.4373
std error	0.158	0.145	0.154	0.166	0.154	0.153	0.157	0.184	0.160	0.159	0.163
t_Vol	1.682	1.889	1.972	0.842	1.248	0.292	2.311	0.996	2.240	2.642	2.688
P value	0.107	0.07	0.062	0.409	0.226	0.773	0.031	0.331	0.036	0.015	0.014

SCR, signal to clutter ratio; Max Blob, largest blob; Weighted, weighted eccentricity; Cutoff, principal component filtering; 3 Deleted, 3 principal components deleted; 4 Delete, 4 principal components deleted; Mod Regular, modified regularization; R, correlation coefficient; R^2, R squared; R^2 adjust, adjusted R squared; D-P Omni, D'Agostino-Pearson Omnibus residual normality test ; S-W, Shapiro-Wilks residual normality test; b_Ecc, eccentricity coefficient; std error, standard error; t_Ecc, eccentricity t-value; b_SCR, SCR coefficient; t_SCR, SCR *t*-value; b_Vol, volume coefficient; t_Vol, volume *t*-value.

Table 3 Matrix of correlation co-efficients (R) between independent variables (eccentricity, SCR, volume)

Variables	Ecc				SCR				Vol			
	Max Blob: 0.35	Max Blob: 0.4	Max Blob: 0.45	Weighted: 0.4	Cutoff: 3 Deleted	Cutoff: 4 Deleted	Mod regular	Z score	Histology	MP-MRI: 0.6	MP-MRI: 0.65	MP-MRI: 0.7
Ecc; Max Blob: 0.35	1	0.957	0.856	0.809	–0.039	–0.194	–0.384	–0.316	–0.523	–0.543	–0.485	–0.484
Ecc; Max Blob: 0.40	0.957	1	0.924	0.786	–0.115	–0.281	–0.466	–0.416	–0.48	–0.523	–0.463	–0.459
Ecc; Max Blob: 0.45	0.856	0.924	1	0.8	–0.176	–0.378	–0.5	–0.481	–0.486	–0.541	–0.476	–0.469
Weighted: 0.4	0.809	0.8	0.786	1	–0.014	–0.416	0.181	–0.353	–0.331	–0.439	–0.35	–0.408
SCR; Cutoff; 3 Deleted	–0.039	–0.115	–0.176	–0.014	1	0.716	0.39	0.39	0.187	–0.227	–0.2	–0.044
SCR; Cutoff; 4 Deleted	–0.194	–0.281	–0.378	–0.263	0.716	1	0.683	0.606	0.079	–0.209	–0.2	–0.149
SCR; Mod regular	–0.384	–0.466	–0.5	–0.181	0.39	0.683	1	0.757	0.179	–0.026	–0.026	–0.118
SCR; Z Score	–0.316	–0.416	0.481	–0.353	0.39	0.606	0.757	1	0.021	–0.024	–0.102	–0.148
Vol; Histology	–0.523	–0.48	–0.486	–0.331	0.187	0.079	0.179	0.021	1	0.609	0.662	0.641
Vol; MP-MRI: 0.60	–0.543	–0.523	–0.541	–0.439	–0.227	–0.209	–0.026	–0.024	0.609	1	0.965	0.887
Vol; MP-MRI: 0.65	–0.485	–0.463	–0.476	–0.35	–0.2	–0.2	–0.026	–0.102	0.662	0.965	1	0.931
Vol; MP-MRI: 0.70	–0.484	–0.459	–0.469	–0.408	–0.044	–0.149	–0.118	–0.148	0.641	0.887	0.931	1

SCR, signal to clutter ratio; Ecc, eccentricity; Vol, volume; Max Blob, largest blob; Weighted, weighted eccentricity; Cutoff, principal component filtering; 3 Deleted, 3 principal components deleted; 4 Delete, 4 principal components deleted; Mod Regular, modified regularization; MP-MRI, multi-parametric magnetic resonance imaging; R, correlation coefficient.

P values >0.05 for the Breusch-Pagan tests.

Figure 2 displays fits to the GS by using eccentricity from the largest blob (ACE threshold =0.40) combined with the SCR with cutoff or filtering of 3 PCs to the GS. *Figure 2A* shows a three-dimensional plot where the orange dots denote the data and the blue dots show the fit. *Figure 2B* shows the plot of the GS against the SCR (filtered out 3 PCs) showing a correlation coefficient of R=0.60, P value =0.0113. *Figure 2C* shows the plot of the GS against the eccentricity (largest blob, ACE threshold =0.40) showing a correlation coefficient of R=–0.658, P value =0.000349. *Figure 2D* shows the plot of the SCR (largest blob, ACE threshold is 0.40) against the eccentricity (largest blob, ACE threshold =0.40) showing a correlation coefficient of R=–0.115, P value =0.583. SCR and eccentricity correlate with GS but not to each other.

Table 2 summarizes metrics for assessing the multivariate fits (Eq. [8]) for MP-MRI-based eccentricity, SCR, and tumor volume measurements to GS. The results from the fitting are also summarized and listed in *Table 2*. SCR related topics and results are also summarized and listed in *Table 2*. Volume related topics and results are also summarized and listed in *Table 2*. The three sets of independent variables use combinations of prostate tumor eccentricity, SCR, and volume. The options for b_Ecc (eccentricity) and b_SCR (SCR) are the same as *Table 1* for two variable fitting. Options for b_Vol include those from histology of whole mount prostatectomy and from applying ACE thresholds (0.6, 0.65, and 0.70) to MP-MRI. The fitted coefficients for the eccentricity, SCR, and volume are b_Ecc, b_SCR, and b_Vol, respectively and are shown

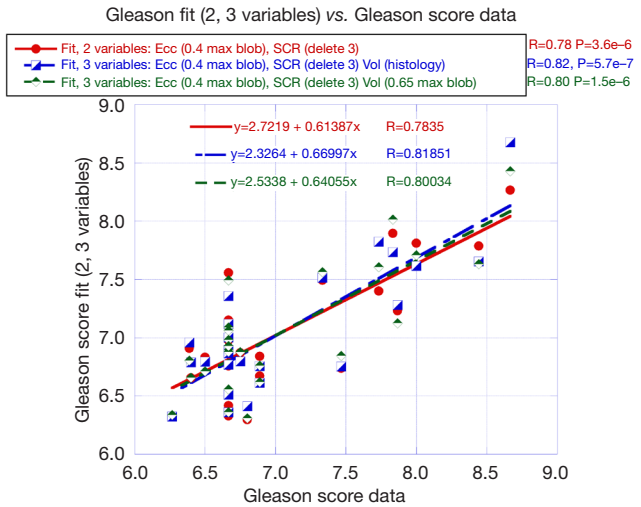

Figure 3 The multivariate fit using ACE/MP-MRI [eccentricity for the largest blob with a 0.4-threshold plus SCR after applying a cutoff of 3 principal components] against data for Gleason score. Volume (histology, MP-MRI) added for three variable fit to Gleason score. SCR, signal to clutter ratio; ACE, adaptive cosine estimator; MP-MRI, multi-parametric magnetic resonance imaging.

along with the standard error for each parameter associated with the fit. The b_Ecc is negative and b_SCR is positive as discussed and shown in *Tables 1*,*2*. The b_Vol is positive, confirming that larger departures of MP-MRI from normal prostate are associated with greater GS. The t statistics for eccentricity (t_Ecc), SCR (t_SCR), and volume (t_Vol) along with P values are displayed in *Table 2*. The magnitude of the t-value t_Ecc is comparable to the t-value t_SCR for all pairs of independent variables. The t_Vol is lower than the t_Ecc and t_SCR except for relatively poor fits (F<10). Correlation coefficient (R), R squared (R^2), adjusted R squared (R^2 adjusted), F-statistic and P value summarize the overall multivariate fit for MP-MRI-based measurements to GS (Eq. [19]).

Table 2 shows the correlation coefficient R and P value from fitting two sets of independent variates in a multivariate analysis (Eq. [19]) for GS ranged from R=0.60 to 0.784 and P value 0.00741 to <0.0001. The t-statistic for the eccentricity is comparable to those from SCR measurements. This MP-MRI analysis processed the 25 patients that took up the contrast material. The residuals in the fits mostly followed a normal distribution as evidenced by the P values for the D'Agostino-Pearson and Shapiro-Wilks tests yielding P values >0.05. The Breusch-Pagan test in all variable combinations finds P values >0.05 and therefore the variables follow homoscedasticity.

Table 3 is a matrix showing the correlation coefficients between the eccentricity, SCR, and volume. The correlation coefficients involving overlap of eccentricity and SCR are also shown. Similarly, the correlation coefficients involving overlap of eccentricity and volume are shown as well as the correlation coefficients involving overlap of volume and SCR are displayed in *Table 3*. As expected, the correlation coefficients within eccentricity, SCR, and volume are larger than correlation coefficients from overlapping components. It should be noted that correlation coefficients involving eccentricity and volume are higher than those for eccentricity and SCR and correlation coefficients for SCR and volume. More correlated independent variables (volume, eccentricity) will combine less effectively in fitting to Gleason score (dependent variable) due to reduced additional, independent information, as seen in *Table 2* and *Figure 3*.

Figure 3 plots the multivariate fit (Eq. [8]) using ACE/MP-MRI (eccentricity for the largest blob with a 0.4-threshold plus SCR after applying a cutoff of 3 PCs) against data for GS. The fit resulted in correlation coefficient of R=0.784 and P value <0.000001. Adding volume, whether from histology or MP-MRI to eccentricity and SCR processing generates R=0.82, P value =5.6e-7, and R=0.80, P value =1.5e-6 and adds little to the fitting to the GS.

Discussion

This study found that combining filtered prostate tumor SCR with the tumor's eccentricity can significantly elevate the correlation coefficient with the patient's GS. For configurations involving eccentricity and SCR that result in lower correlation with GS, adding MP-MRI derived tumor volume can elevate the correlation coefficient with GS. The optimal tumor eccentricity and inferred volume from the largest blob depend on the ACE threshold. Weighted eccentricity averages over all blobs correlates significantly with GS, but not as highly as those from the largest blob. The optimal SCR requires filtering out the noise by removing a number of PCs from the covariance matrix. A modified regularization applied to the covariance matrix performs well, albeit not as well as the filtered application. This study confirmed a previous study (20) that eccentricity related independent variable correlated better with GS and attained higher t-values in multivariate fits than MP-MRI

derived tumor volume measurements. The histology derived tumor volume measurements consistently helped achieve higher correlation with GS in multivariate fits than the MP-MRI. It may be possible to combine histology and MP-MRI to predict GS but its utility is limited due to the invasive nature of whole mount prostatectomy relative to MRI.

The relationship among the independent variables (eccentricity, SCR, volume) was examined to see if they were truly independent. From *Table 3*, the correlation coefficients involving volume and eccentricity are relatively high. The higher correlation coefficient means that adding volume to the GS (dependent variable) fit should yield little additional, independent information and minimal improvement in fitting as seen in *Table 2* and *Figure 3*. However, the reported correlation coefficients in *Table 3* between eccentricity and SCR and volume and SCR are low, showing little correlation among those sets of variables.

The metrics examined in this study (eccentricity, SCR, volume) are generated non-invasively by quantitatively analyzing spatially registered multi-parametric MRI. Generating and adding these indicators to predict clinical outcome should benefit the patient by reducing the burden and potential side effects on the patient. In addition, using eccentricity and SCR can aid the radiologist in assessing MRI to determine the interpretation of MRI and clinical direction in proscribing patient therapy and reducing variability among radiologists in generating PI-RADS scoring (16). The histology derived tumor volume adds greater predictive value for GS than from tumor volume inferred from MP-MRI. It is hoped that future research will improve the MP-MRI generated tumor volume.

In addition to this study of fitting of individual components, the GS was fit using multivariable regression with of two and three variables that incorporated Analysis of Variance (ANOVA) and Three-Way ANOVA when appropriate. This parallel study, although not shown, was quite extensive. However, the results involving the same variables (eccentricity, volume, SCR) yielded essentially the same results as this study regarding the relative strength of the fits and the correlation among the variables. Additional data analysis confirmed the analysis discussed in this manuscript and added little new information. For simplicity, the multivariable fit analysis was not included in this paper.

The high correlation of GS and MP-MRI metrics such as filtered SCR and eccentricity exceeds those from current standard approaches such as PSA, age etc. Although the Pearson correlation coefficients between z-score, SCR and GS are not close to 1.0, they are statistically significant with low P values. To provide a reference point, the connection between PSA and GS ranges finds the Pearson correlation coefficient (R) varies from R=0.59 (8) to R=0.43–0.46 (9) and a P value =0.75, showing no statistical significance (7). The PI-RADS and GS relationship also varies among studies. Bastian-Jordan (15) showed the incidence of clinically significant disease for different PIRADS grades. PI-RADS score was not associated with significant differences regarding GS distribution within the target (14). However, the PI-RADS score significantly correlated with postoperative extracapsular extension, lymphovascular invasion, and seminal vesicle involvement were significant (P<0.001, P=0.032, and P=0.007, respectively) (13).

If additional studies analyzing greater patient numbers and prospective analyses confirm combining SCR/Z-scores, eccentricity with metadata such as age, family history, PSA etc. significantly correlate with GS, then clinical implementation is feasible. The biggest issue is generating spatially registered hypercubes from MP-MRI in a timely manner. Software development should enable autonomous spatial registration that should reduce time to assemble the hypercubes. Identifying tumors by the radiologist to generate tumor signature is simplified for spatial-registered hypercubes through color processing discussed in earlier studies (17-21).

This study has some limitations. The patients in this stud were prospectively enrolled, but originated from a single institution (NIH). Clinical implementation variations were therefore not examined and the effects of variation on this analysis are uncertain. In addition, this is a retrospective analysis of the data and may be subject to biases. Lastly, the dataset comprised only 25 patients. Although a small number of patients were assessed, consecutive patients were analyzed to minimize potential bias, and nevertheless highly statistically significant P values were achieved, showing potential clinical value of this approach.

Conclusions

Combining prostate tumors eccentricity with its processed SCR is highly correlated with GS. Adding volume marginally improved the multivariate fit.

Acknowledgments

Funding: None.

Footnote

Reporting Checklist: The authors have completed the TRIPOD reporting checklist. Available at https://qims.amegroups.com/article/view/10.21037/qims-21-1092/rc

Conflicts of Interest: All authors have completed the ICMJE uniform disclosure form (available at https://qims.amegroups.com/article/view/10.21037/qims-21-1092/coif). The authors have no conflicts of interest to declare.

Ethical Statement: The authors are accountable for all aspects of the work in ensuring that questions related to the accuracy or integrity of any part of the work are appropriately investigated and resolved. The study was conducted in accordance with the Declaration of Helsinki (as revised in 2013). This retrospectively designed, single institution study was approved by the NIH Institutional Review Board, and was compliant with the Health Insurance Portability and Accountability Act. And individual consent for this retrospective analysis was waived.

References

1. Dall'Era MA, Albertsen PC, Bangma C, Carroll PR, Carter HB, Cooperberg MR, Freedland SJ, Klotz LH, Parker C, Soloway MS. Active surveillance for prostate cancer: a systematic review of the literature. Eur Urol 2012;62:976-83.
2. Shariat SF, Karakiewicz PI, Roehrborn CG, Kattan MW. An updated catalog of prostate cancer predictive tools. Cancer 2008;113:3075-99.
3. Martin NE, Mucci LA, Loda M, Depinho RA. Prognostic determinants in prostate cancer. Cancer J 2011;17:429-37.
4. Ho R, Siddiqui MM, George AK, Frye T, Kilchevsky A, Fascelli M, Shakir NA, Chelluri R, Abboud SF, Walton-Diaz A, Sankineni S, Merino MJ, Turkbey B, Choyke PL, Wood BJ, Pinto PA. Preoperative Multiparametric Magnetic Resonance Imaging Predicts Biochemical Recurrence in Prostate Cancer after Radical Prostatectomy. PLoS One 2016;11:e0157313.
5. May M, Siegsmund M, Hammermann F, Loy V, Gunia S. Visual estimation of the tumor volume in prostate cancer: a useful means for predicting biochemical-free survival after radical prostatectomy? Prostate Cancer Prostatic Dis 2007;10:66-71.
6. Poulakis V, Witzsch U, de Vries R, Emmerlich V, Meves M, Altmannsberger HM, Becht E. Preoperative neural network using combined magnetic resonance imaging variables, prostate-specific antigen, and gleason score for predicting prostate cancer biochemical recurrence after radical prostatectomy. Urology 2004;64:1165-70.
7. Gurumurthy D, Maggad R, Patel S. Prostate carcinoma: correlation of histopathology with serum prostate specific antigen. Science Journal of Clinical Medicine 2015;4:1-5.
8. Ngwu PE, Achor GO, Eziefule VU, Orji JI, Alozie FT. Correlation between Prostate Specific Antigen and Prostate Biopsy Gleason Score. Annals of Health Research 2019;5(2). DOI: https://doi.org/10.30442/ahr.0502-26-56.
9. Zivkovic S. Correlation between prostate-specific antigen and histopathological difference of prostate carcinoma. Arch Oncol 2004;12:148-51.
10. Gleason DF, Mellinger GT. Prediction of prognosis for prostatic adenocarcinoma by combined histological grading and clinical staging. J Urol 1974;111:58-64.
11. Weinreb JC, Barentsz JO, Choyke PL, Cornud F, Haider MA, Macura KJ, Margolis D, Schnall MD, Shtern F, Tempany CM, Thoeny HC, Verma S. PI-RADS Prostate Imaging - Reporting and Data System: 2015, Version 2. Eur Urol 2016;69:16-40.
12. Wang L, Hricak H, Kattan MW, Chen HN, Kuroiwa K, Eisenberg HF, Scardino PT. Prediction of seminal vesicle invasion in prostate cancer: incremental value of adding endorectal MR imaging to the Kattan nomogram. Radiology 2007;242:182-8.
13. Kızılay F, Çelik S, Sözen S, Özveren B, Eskiçorapçı S, Özgen M, Özen H, Akdoğan B, Aslan G, Narter F, Çal Ç, Türkeri L; Members of Urooncology Association. Correlation of Prostate-Imaging Reporting and Data Scoring System scoring on multiparametric prostate magnetic resonance imaging with histopathological factors in radical prostatectomy material in Turkish prostate

cancer patients: a multicenter study of the Urooncology Association. Prostate Int 2020;8:10-5.
14. Slaoui H, Neuzillet Y, Ghoneim T, Rouanne M, Abdou A, Lugagne-Delpon PM, Scherrer A, Radulescu C, Delancourt C, Molinié V, Lebret T. Gleason Score within Prostate Abnormal Areas Defined by Multiparametric Magnetic Resonance Imaging Did Not Vary According to the PIRADS Score. Urol Int 2017;99:156-61.
15. Bastian-Jordan M. Magnetic resonance imaging of the prostate and targeted biopsy, Comparison of PIRADS and Gleason grading. J Med Imaging Radiat Oncol 2018;62:183-7.
16. Smith CP, Harmon SA, Barrett T, Bittencourt LK, Law YM, Shebel H, An JY, Czarniecki M, Mehralivand S, Coskun M, Wood BJ, Pinto PA, Shih JH, Choyke PL, Turkbey B. Intra- and interreader reproducibility of PI-RADSv2: A multireader study. J Magn Reson Imaging 2019;49:1694-703.
17. Mayer R, Simone CB 2nd, Skinner W, Turkbey B, Choykey P. Pilot study for supervised target detection applied to spatially registered multiparametric MRI in order to non-invasively score prostate cancer. Comput Biol Med 2018;94:65-73.
18. Mayer R, Simone CB 2nd, Turkbey B, Choyke P. Algorithms applied to spatially registered multi-parametric MRI for prostate tumor volume measurement. Quant Imaging Med Surg 2021;11:119-32.
19. Mayer R, Simone CB 2nd, Turkbey B, Choyke P. Correlation of prostate tumor eccentricity and Gleason scoring from prostatectomy and multi-parametric-magnetic resonance imaging. Quant Imaging Med Surg 2021;11:4235-44.
20. Mayer R, Simone CB 2nd, Turkbey B, Choyke P. Prostate tumor eccentricity predicts Gleason score better than prostate tumor volume. Quant Imaging Med Surg 2022;12:1096-108.
21. Mayer R, Simone CB 2nd, Turkbey B, Choyke P. Development and testing quantitative metrics from multi-parametric magnetic resonance imaging that predict Gleason score for prostate tumors. Quant Imaging Med Surg 2022;12:1859-70.
22. Choyke P, Turkbey B, Pinto P, Merino M, Wood B. Data From PROSTATE-MRI. The Cancer Imaging Archive. Available online: http://doi.org/10.7937/K9/TCIA.2016.6046GUDv, 2016.
23. Clark K, Vendt B, Smith K, Freymann J, Kirby J, Koppel P, Moore S, Phillips S, Maffitt D, Pringle M, Tarbox L, Prior F. The Cancer Imaging Archive (TCIA): maintaining and operating a public information repository. J Digit Imaging 2013;26:1045-57.
24. Shah V, Pohida T, Turkbey B, Mani H, Merino M, Pinto PA, Choyke P, Bernardo M. A method for correlating in vivo prostate magnetic resonance imaging and histopathology using individualized magnetic resonance-based molds. Rev Sci Instrum 2009;80:104301.
25. Turkbey B, Mani H, Shah V, Rastinehad AR, Bernardo M, Pohida T, Pang Y, Daar D, Benjamin C, McKinney YL, Trivedi H, Chua C, Bratslavsky G, Shih JH, Linehan WM, Merino MJ, Choyke PL, Pinto PA. Multiparametric 3T prostate magnetic resonance imaging to detect cancer: histopathological correlation using prostatectomy specimens processed in customized magnetic resonance imaging based molds. J Urol 2011;186:1818-24.
26. Turkbey B, Pinto PA, Mani H, Bernardo M, Pang Y, McKinney YL, Khurana K, Ravizzini GC, Albert PS, Merino MJ, Choyke PL. Prostate cancer: value of multiparametric MR imaging at 3 T for detection--histopathologic correlation. Radiology 2010;255:89-99.
27. Tofts PS, Brix G, Buckley DL, Evelhoch JL, Henderson E, Knopp MV, Larsson HB, Lee TY, Mayr NA, Parker GJ, Port RE, Taylor J, Weisskoff RM. Estimating kinetic parameters from dynamic contrast-enhanced T(1)-weighted MRI of a diffusable tracer: standardized quantities and symbols. J Magn Reson Imaging 1999;10:223-32.
28. Tofts PS. T1-weighted DCE Imaging Concepts: Modelling, Acquisition and Analysis. Magnetom Flash 2010;3:31-9.
29. Jain AK. Fundamentals of Digital Image Processing. Upper Saddle River, NJ: Prentice Hall, 1989.
30. Richards JA, Jia X. Remote Sensing Digital Image Analysis. New York: Springer-Verlag, 1999.
31. Manolakis D, Shaw G. Detection algorithms for hyperspectral imaging applications. IEEE Sign. Processing Magazine 2002;19:29-43.
32. Kreyszig E. Advanced Engineering Mathematics (Fourth ed). Hoboken: Wiley, 1979.
33. Strang G. Linear algebra and its applications (Fourth ed). Belmont, CA, Thomson, Brooks/Cole, 2006.
34. Chen G, Qian S. Denoising of Hyperspectral Imagery Using Principal Component Analysis and Wavelet Shrinkage. IEEE Transactions on Geoscience and Remote Sensing 2011;49:973-80.
35. Friedman JH. Regularized Discriminant Analysis. J Amer

Stat Assoc 1989;84:165-75.
36. Mardia KV, Kent JT, Bibby JM. Multivariate Analysis. Academic Press, 1979.
37. Kmenta J. Elements of Econometrics (Second ed). New York: Macmillan, 1986.
38. Walpole RE. Probability & statistics for engineers & scientists. Myers, H. Raymond. (7th ed). New Delhi: Pearson, 2006.
39. Chatterjee S, Simonoff J. Handbook of Regression Analysis. Hoboken: John Wiley & Sons, 2013.

Cite this article as: Mayer R, Turkbey B, Choyke P, Simone CB 2nd. Combining and analyzing novel multi-parametric magnetic resonance imaging metrics for predicting Gleason score. Quant Imaging Med Surg 2022;12(7):3844-3859. doi: 10.21037/qims-21-1092

